Supporting Information

Multifunctional nitrogen-rich "brick-and-mortar" carbon as high performance supercapacitor electrodes and oxygen reduction electrocatalysts

Dingshan Yu,[a] Kunli Goh,[a] Li Wei,[a] Hong Wang,[a] Qiang Zhang,[b] Wenchao Jiang,[a] Rongmei Si,[a] and Yuan Chen*[a]

a. School of Chemical and Biomedical Engineering, Nanyang Technological University, 62 Nanyang Drive, Singapore 637459

b. Department of Chemical Engineering, Tsinghua University, Beijing 100084, P. R. China

E-mail: chenyuan@ntu.edu.sg; Fax: +65-65156046; Tel: +65-63168939

Table S1. Comparison of the capacitive performance of N-enriched carbon materials in aqueous electrolytes in literatures.

N-enriched carbon materials	S_{BET} (m^2 g^{-1})	Electrolyte	C_g (F/g)	Ref.
N-rich hydrothermal carbon from D-glucosamine	598	6M KOH	220	16
		1M H_2SO_4	300	
Aminated Graphene Honeycombs	666	6M KOH	192	33
B, N codoped carbon using ionic liquid $C_{16}mimBF_4$	376	6M KOH	247	15
N-rich carbon from the polyvinylidene fluoride (PVDF)/melamine mixture	560	1M H_2SO_4	310	34
N-rich composite of CNTs and carbon derived from melamine	400	1M H_2SO_4	160	35
Activated and N-rich CNT	568	7M KOH	58	36
N doped porous carbon fiber	562	6M KOH	202	37
ammoxidized coals	660-1200	4M H_2SO_4	175	38
		7M KOH	145	
templated mesoporous N-enriched carbon materials	800	1M H_2SO_4	201	39
N-enriched carbon with large mesopores	1330	5M H_2SO_4	211	40
O-rich carbons from seaweed polymer	173	5M H_2SO_4	198	41
N-enriched carbon from melamine–mica	6-86	1M H_2SO_4	115	42
		6M KOH	198	
CNT/N-rich carbon composite	157	1M H_2SO_4	100	43
Functionalized three-dimensional hierarchical porous carbon	2870	6M KOH	318	44
N-doped activated graphene	705	6M KOH	420	45
This work	957	6M KOH	361	

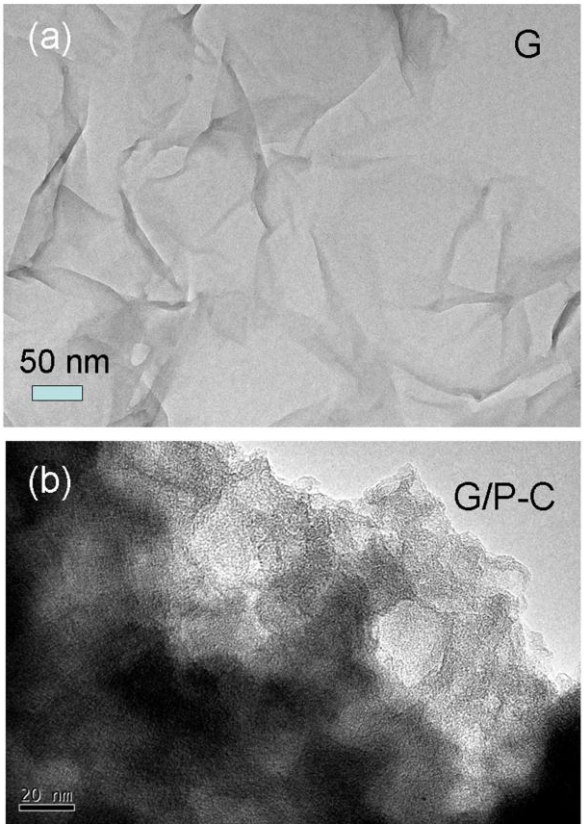

Fig. S1 TEM images of the G and G-16/P-C samples

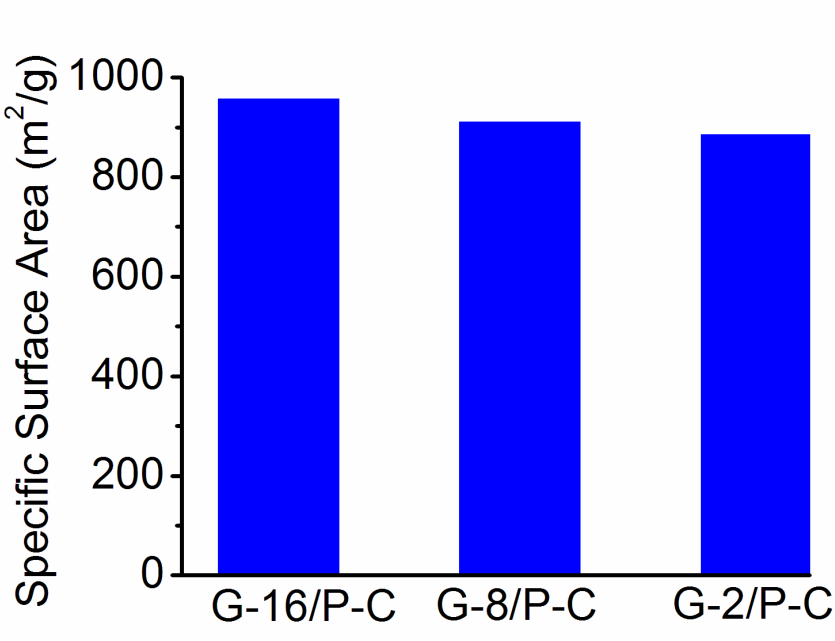

Fig. S2 Comparison of specific surface area from different composite carbon samples.

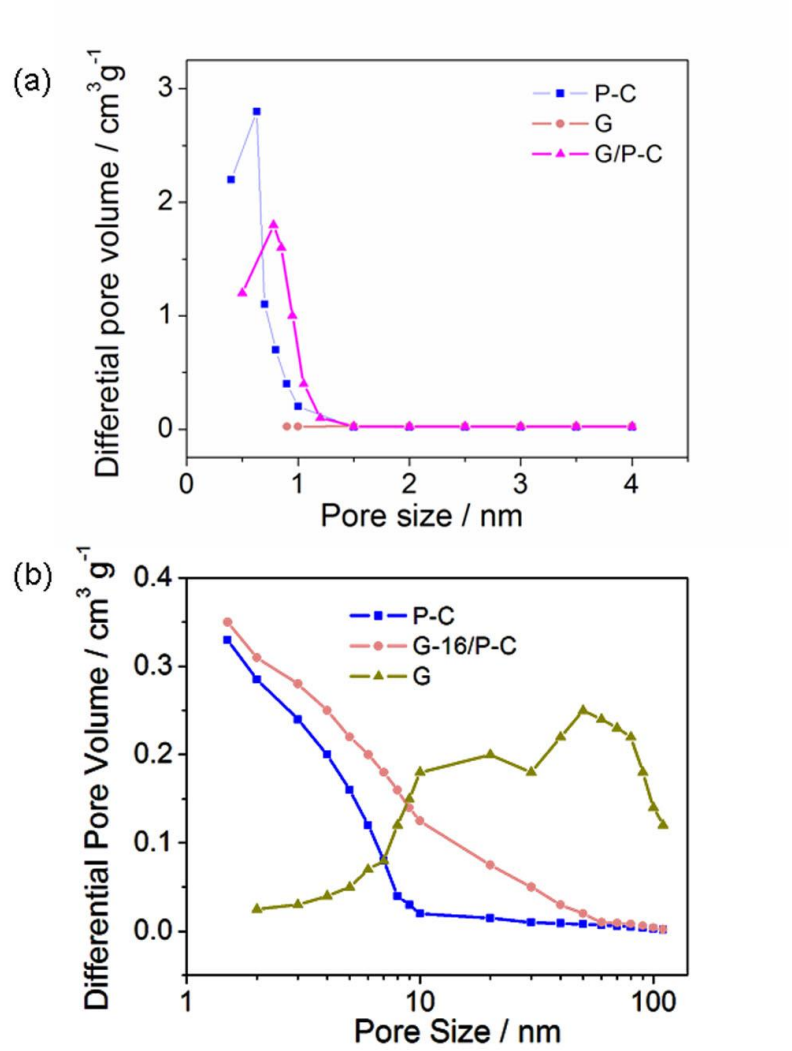

Fig. S3 (a) Micropore size distribution, and (b) mesopore size distribution of G, P-C, and G-16/P-C

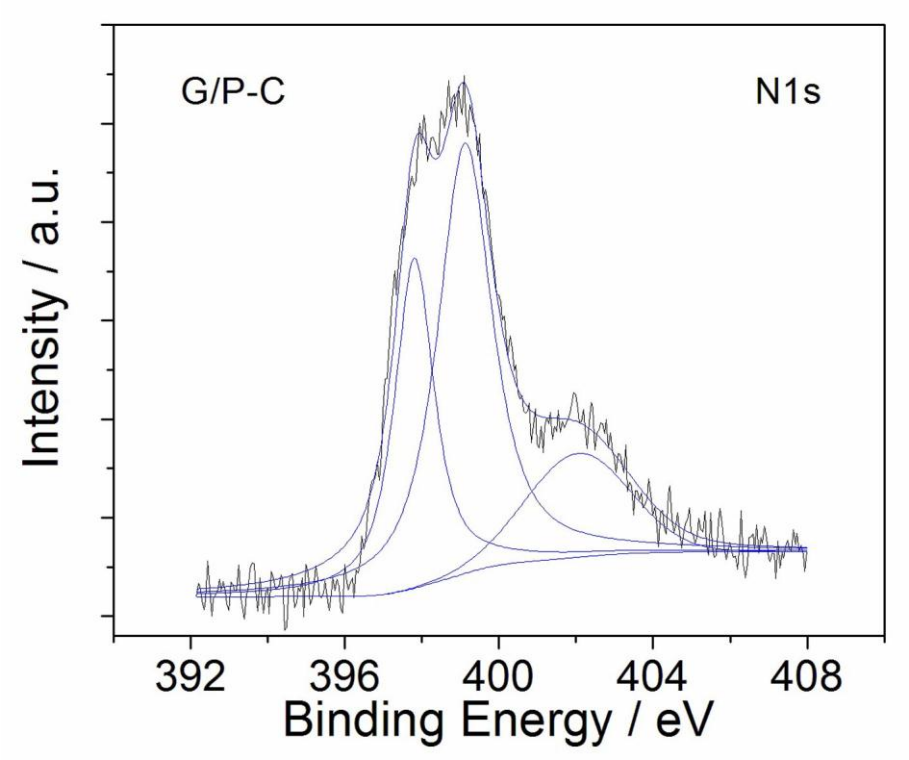

Fig. S4 High resolution N1s X-ray photoelectronic spectrum of G/P-C.

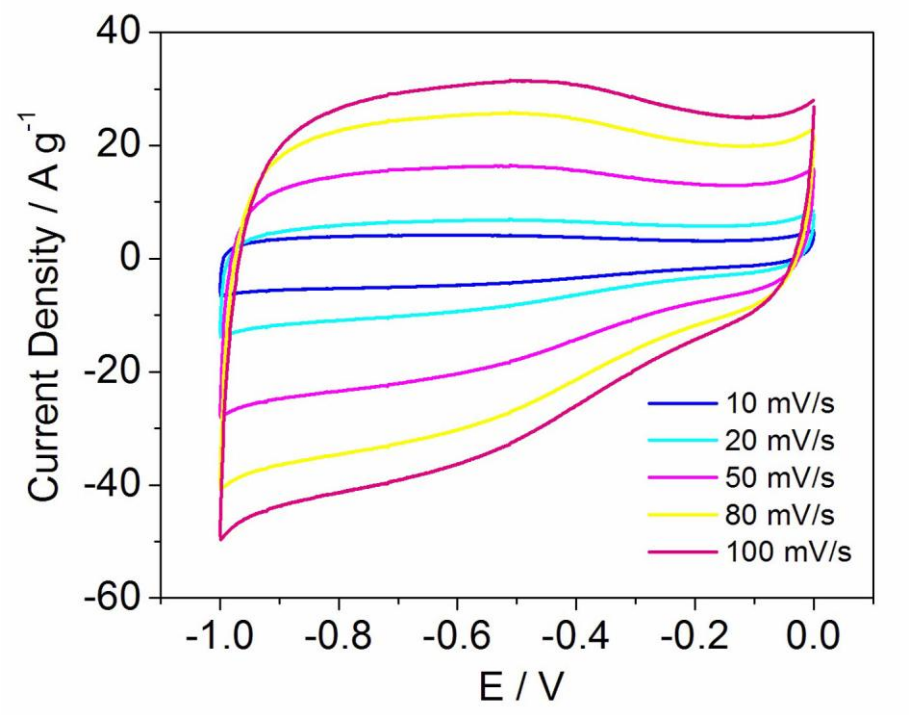

Fig. S5 CV curves of G/P-C in 6 M KOH at different scan rates.

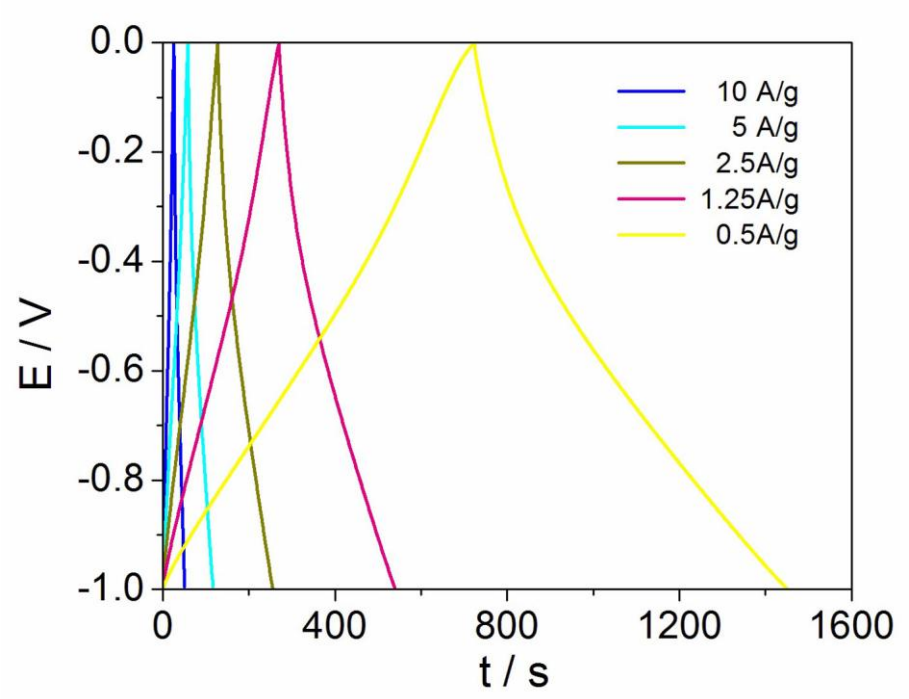

Fig. S6 Galvanostaic charge-discharge curves of G/P-C in 6 M KOH at various current densities.

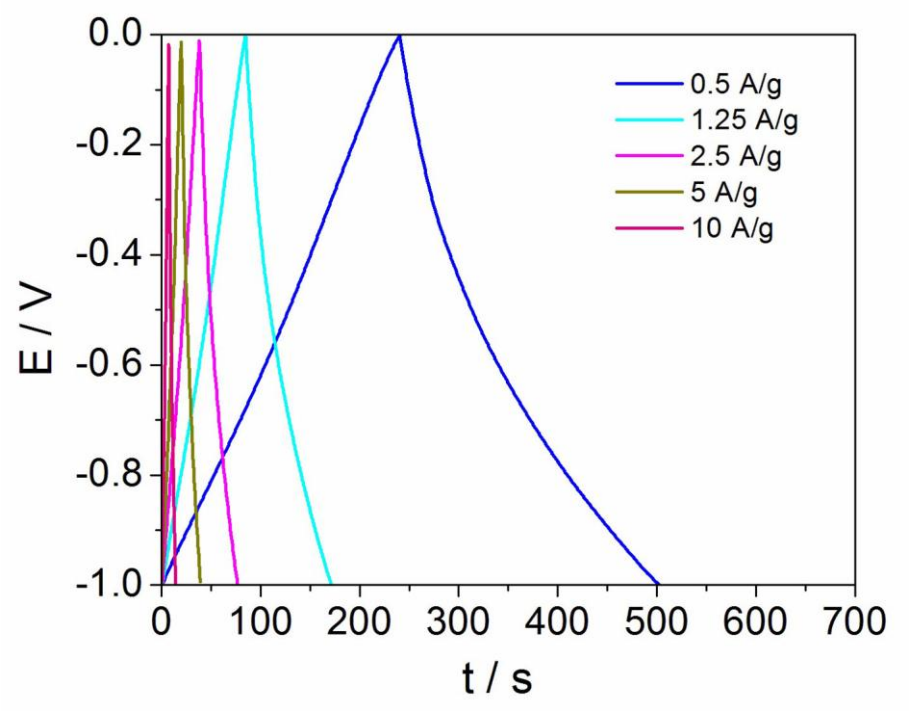

Fig. S7 Galvanostaic charge-discharge curves of G in 6 M KOH at various current densities.

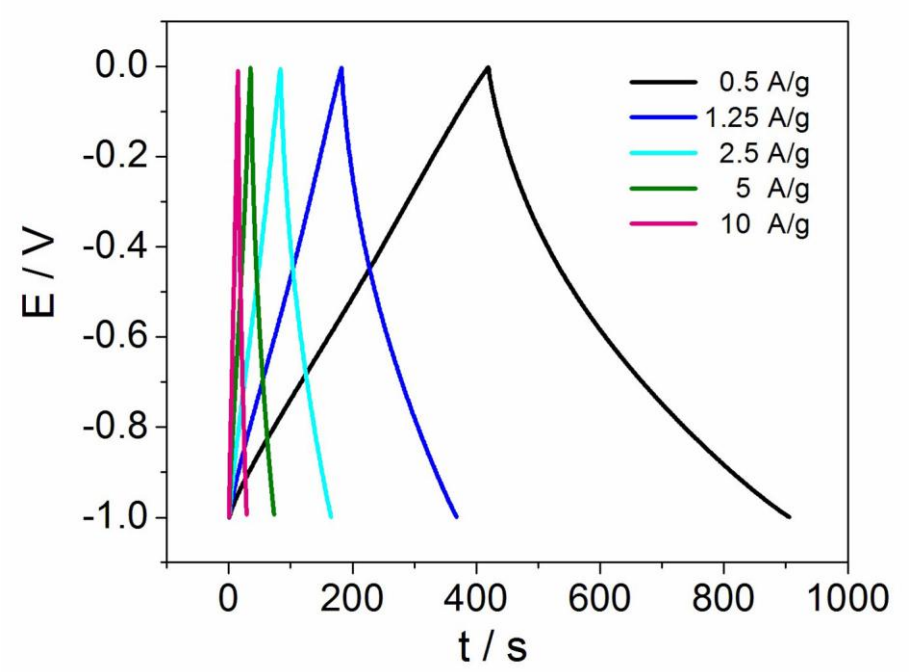

Fig. S8 Galvanostaic charge-discharge curves of P-C in 6 M KOH at various current densities.

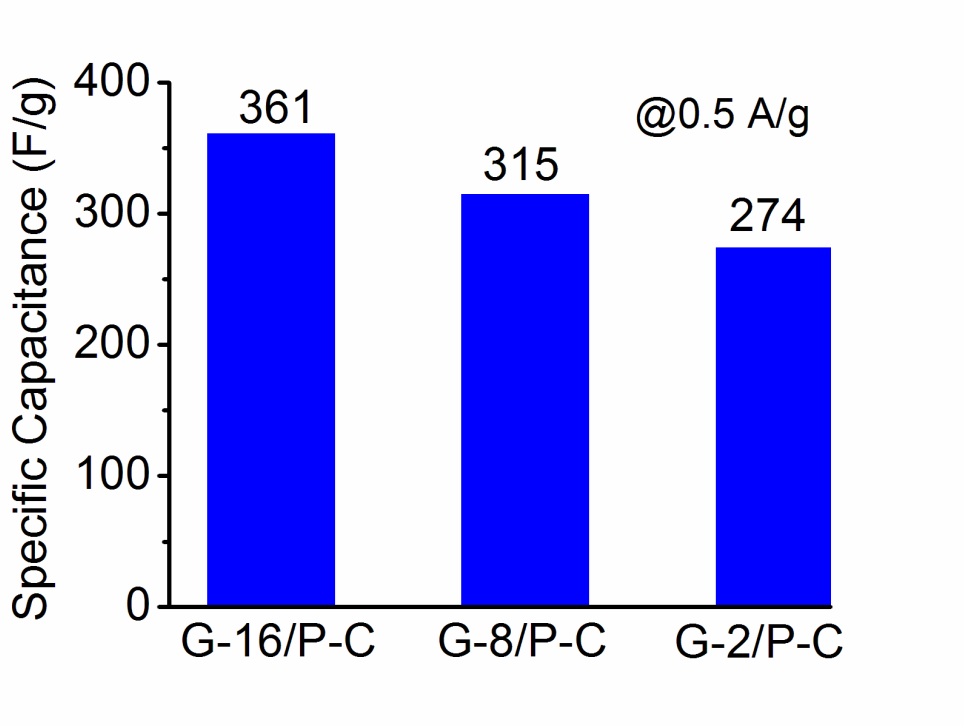

Fig. S9 Comparision of specific capacitance from different composite carbon samples.

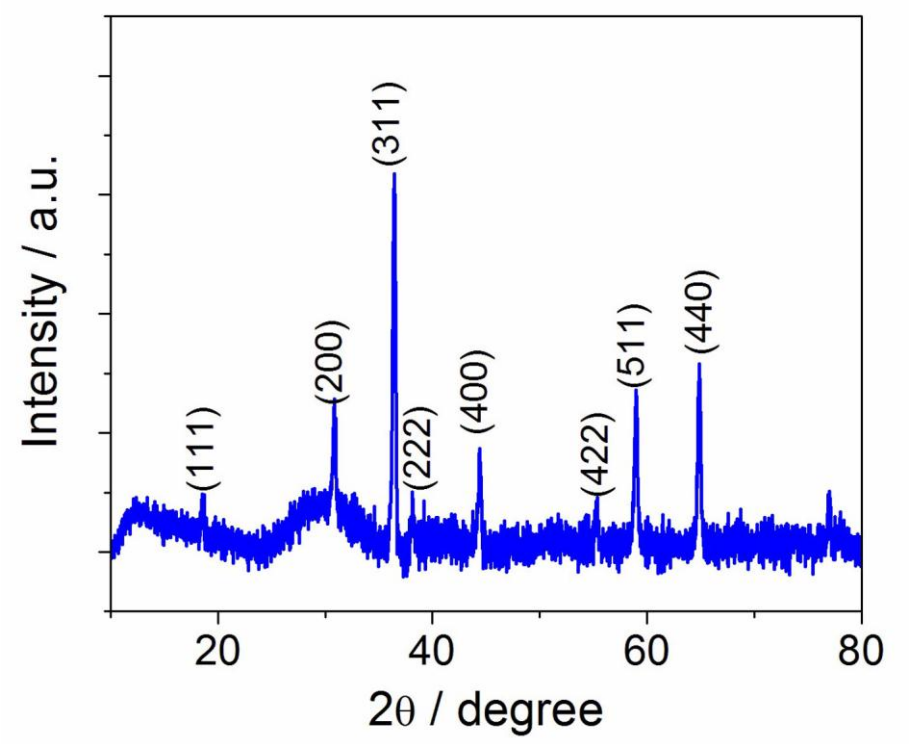

Fig. S10 X-ray diffraction pattern of porous Co_3O_4 nanorods.

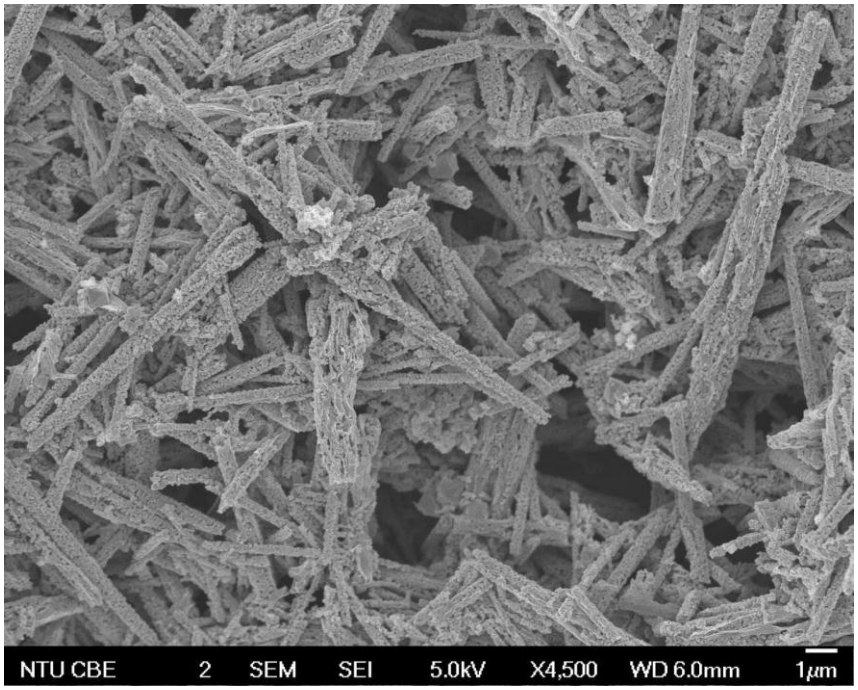

Fig. S11 A typical SEM image of porous Co_3O_4 nanorods.

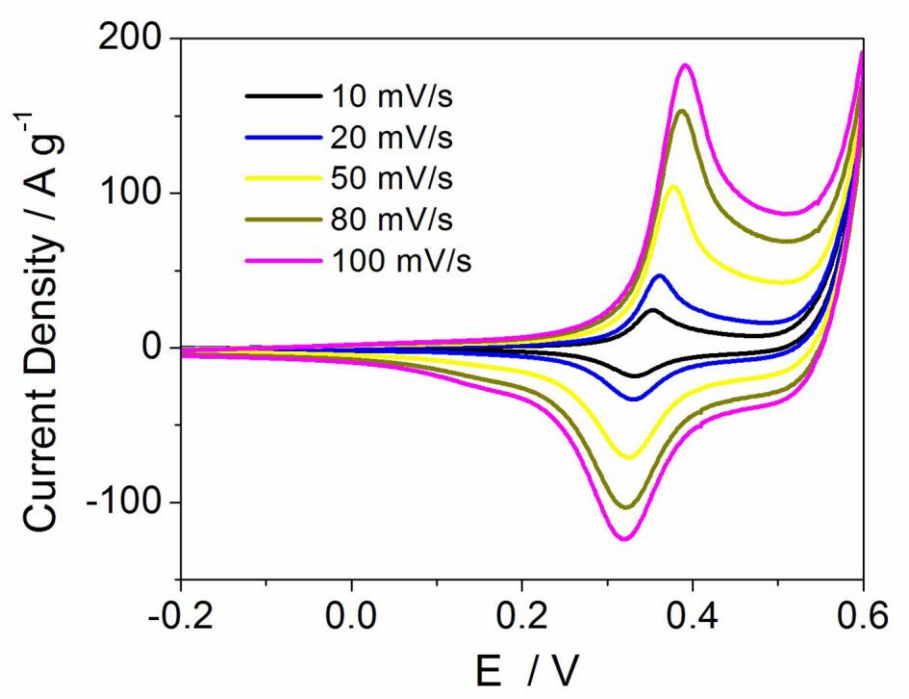

Fig. S12 CV curves of porous Co_3O_4 nanorods in 6 M KOH at different scan rates.

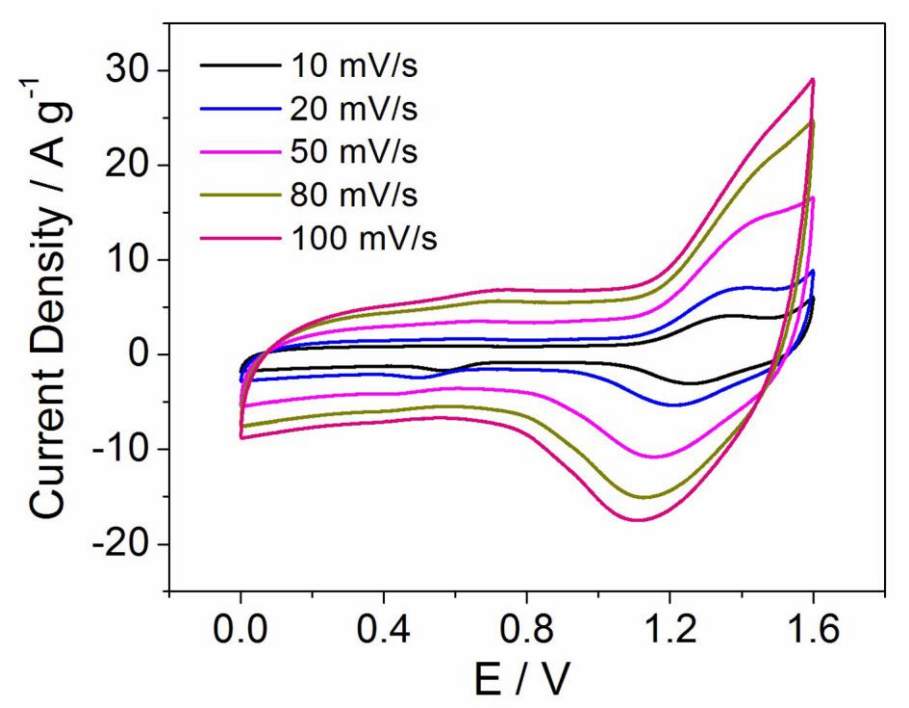

Fig. S13 CV curves of asymmetric G/P-C//Co_3O_4 supercapacitors at different scan rates with a potential window of 1.6 V in 6 M KOH.

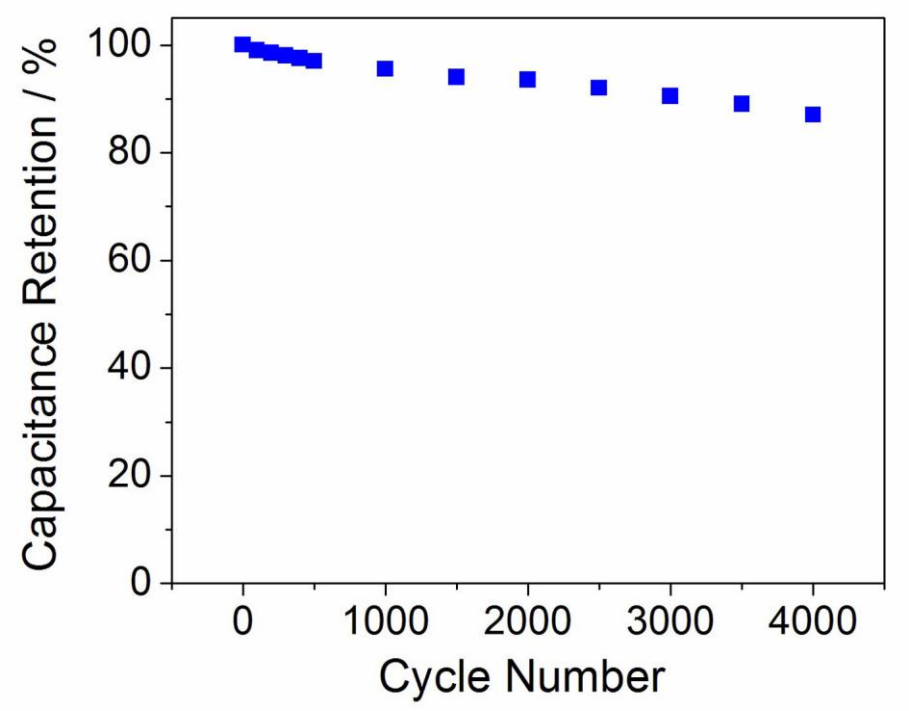

Fig. S14 The cycle performance of asymmetric G/P-C//Co_3O_4 supercapacitors at the charge/discharge current density of 5 A g^{-1} for 4000 cycles.

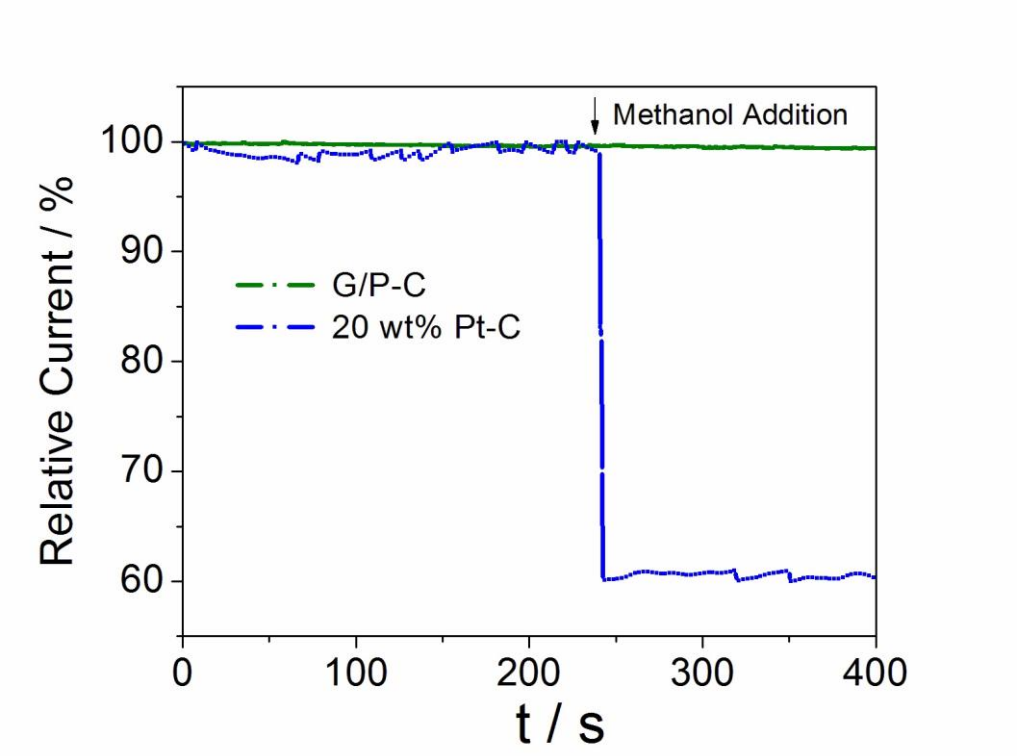

Fig. S15 Chronoamperometric responses for ORR of the G/P-C/GC electrode and the 20 wt% Pt−C/GC electrode upon addition of 1 M methanol after about 230 s at −0.25 V.